



Open Archive Toulouse Archive Ouverte





OATAO is an open access repository that collects the work of Toulouse researchers and makes it freely available over the web where possible

This is an author's version published in: <http://oatao.univ-toulouse.fr/25721>

Official URL:

<https://doi.org/10.1109/TIA.2014.2354405>

To cite this version:

Nguyen, Kien Long  and Pateau, Olivier and Caux, Stéphane  and Egalon, Julie  and Maussion, Pascal  *Robustness of a resonant controller for a multiphase induction heating system.* (2015) IEEE Transactions on Industry Applications, 51 (1). 73-81. ISSN 0093-9994.

Any correspondence concerning this service should be sent to the repository administrator: tech-oatao@listes-diff.inp-toulouse.fr

Robustness of a Resonant Controller for a Multiphase Induction Heating System

Kien Long Nguyen, Olivier Pateau, Stéphane Caux, *Member, IEEE*,
Pascal Maussion, *Member, IEEE*, and Julie Egalon

Abstract—This paper presents a robustness study of the current control scheme for a multiphase induction heating system. Resonant control has been chosen in order to achieve a perfect current reference tracking in the inductors with different solutions from the literature. A simplified model of the system is given; it is based on data extracted from finite-element software, including a model of the energy transfer between the dc source and the currents. The metal sheet resistivity will change with temperature, inducing some modifications in the system parameters. These disturbances will be rejected by the resonant controllers whose pole and zero variations are investigated. In addition, the tuning method for the resonant controllers is detailed when the sampling frequency/switching frequency ratio is very low. Some specific stability zones are defined for the resonant controller gains. The application is currently developed on a test bench devoted to disc induction heating.

Index Terms—Current control, electromagnetic induction, induction heating, metal industry, multiphase, resonant control.

I. INTRODUCTION

INDUCTION heating is expanding in metal industries for applications such as melting, annealing, welding, heat treatment, drying, or merging. The heating speed, its high power density, the possibility of heating inaccessible pieces, and its flexibility are all benefits. Moreover, the association to power electronic devices generally allows a precise control of the heat profile in the load. The classical solutions focus on a single inductor. Some IH generators involve multiple inductors [1], [2] with moving magnetic screens and flux concentrators such as in Fig. 1. Moreover, power electronics can provide a flexible so-

K. L. Nguyen, S. Caux, and P. Maussion are with the Université de Toulouse, 31042 Toulouse, France, with the Institut National Polytechnique de Toulouse (INPT), Université Paul Sabatier (UPS), 31062 Toulouse, France, and also with the Laboratoire PLASMA et Conversion d'Énergie (LAPLACE), Centre National de la Recherche Scientifique (CNRS), École Nationale Supérieure d'Électronique, d'Électrotechnique, d'Informatique, d'Hydraulique et des Télécommunications (ENSEEIH), 31071 Toulouse, France (e-mail: kienlong.nguyen@laplace.univ-tlse.fr; stephane.caux@laplace.univ-tlse.fr; pascal.maussion@laplace.univ-tlse.fr).

O. Pateau is with the Eco-Efficiency and Industrial Process Department, Electricité de France (EDF), 77818 Moret sur Loing, France (e-mail: olivier.pateau@edf.fr).

J. Egalon is with Betem Midi Pyrénées, 31200 Toulouse Cedex, France (e-mail: julie.egalon@laplace.univ-tlse.fr).

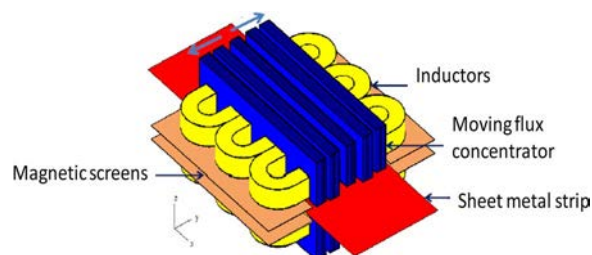


Fig. 1. Transverse flux induction heating with moving parts.

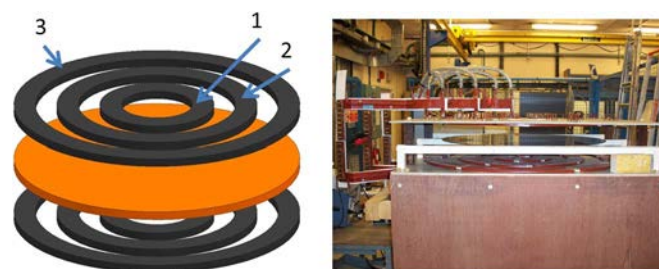


Fig. 2. Three inductors in a face-to-face configuration.

lution with advantages in terms of cost and performance. Most methods for controlling the power density or the temperature in the load have been presented on single inductor heating and a very few for multiinductor systems.

In [3], each inductor is powered by its own power supply constituted by a diode rectifier, a filter, an inverter, and an FPGA. A study of the temperature control is present but does not take into account the coupling between the inductors. References [4] and [5] incorporate the structures of [6] to achieve control of the currents in the inductors. For this, two methods are proposed. The first one [4] deals with the regulation of the amplitude and phase currents. The second one [5] focuses on the real and imaginary parts of the currents. For the last one, decoupling methods are implemented. Currents are in phase, and selected structures are using decoupling transformers between two inductors side by side. In order to keep a constant inductor current with no phase variation and no magnitude oscillation, [7] proposes a combination of pulse frequency modulation and phase-locked loop in a single phase. The analysis of the closed loop proves the stability of the system, depending on PI regulator parameters. Comparatively, the next parts will describe our solutions, in terms of device organization and current control method. The emphasis is put on the consequences of parameter variations due to temperature rise in the disc which are considered as disturbances. Properly tuned resonant control on each of the three phases will reject these disturbances in order to achieve a satisfying control of the inductor currents.

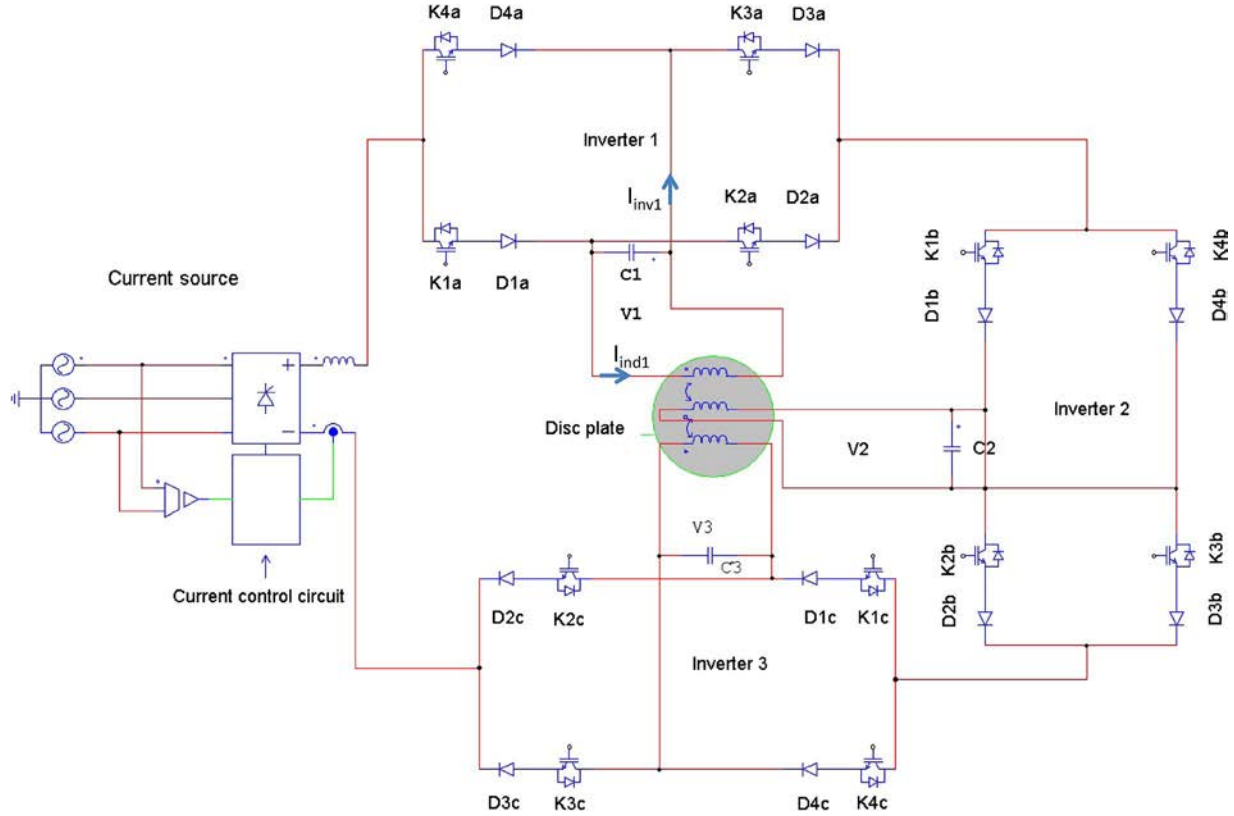


Fig. 3. Whole system schematic with inverters, controlled-current source, capacitors, and coupled inductor.

II. MODEL OF A THREE-PHASE INDUCTION HEATING SYSTEM

The system consists of three inductor coils (Fig. 2) organized face to face in a transverse flux configuration. The workpiece to be heated is a disc plate situated inside the coils. This test bench was initially developed to test different ideas such as the multiphase supply concept and the optimization of the current references as previously described in [8]–[10]. The whole system is supplied by three resonant current inverters, presented in Fig. 3. For modeling and control purposes, it can be represented by a three-phase electrical circuit including the material to be heated where flowed by a short-circuit current.

After some simple calculations presented in [8] and [9], a matrix description of the system is given in (1), where sinusoidal currents I_1 , I_2 , and I_3 feed the three coils. An impedance matrix $[Z_{ij}]$ links the three inductor voltages V_1 , V_2 , and V_3 to the associated inductor currents I_1 , I_2 , and I_3 . Different elements can be found in the real and imaginary parts of the Z_{ij} terms: the self-resistances and inductances of the coils, the coupling terms inductors-load, and the mutual inductance between the inductors

$$\begin{bmatrix} \bar{V}_1 \\ \bar{V}_2 \\ \bar{V}_3 \end{bmatrix} = \begin{bmatrix} \bar{Z}_{11} & \bar{Z}_{12} & \bar{Z}_{13} \\ \bar{Z}_{21} & \bar{Z}_{22} & \bar{Z}_{23} \\ \bar{Z}_{31} & \bar{Z}_{32} & \bar{Z}_{33} \end{bmatrix} \begin{bmatrix} I_1 \\ I_2 \\ I_3 \end{bmatrix} \quad (1)$$

$$\bar{Z}_{ii} = \left(R_i + \frac{\omega^2 M_{i4}^2 R_4}{R_4^2 + (\omega L_4)^2} \right) + j\omega \left(L_i + \frac{\omega^2 M_{i4}^2 L_4}{R_4^2 + (\omega L_4)^2} \right) \quad (2)$$

$$\bar{Z}_{ij} = \left(\frac{\omega^2 M_{i4} M_{4j} R_4}{R_4^2 + (\omega L_4)^2} \right) + j\omega \left(M_{ij} + \frac{\omega^2 M_{i4} M_{4j} L_4}{R_4^2 + (\omega L_4)^2} \right) \quad (3)$$

where

- $M_{i,4}$ coupling terms between the inductors i and the material to be heated (load);
- R_i, L_i self-resistance and inductance for inductor i ;
- R_4, L_4 disc plate resistance and inductance;
- M_{ij} mutual inductance between inductors i and j .

As shown by (2) and (3), Z_{ij} real and imaginary parts are both nonlinear, with regard to the frequency ω and the temperature. Indeed, parameter R_4 that models the material resistance of the stainless steel disc is temperature dependent. Numerical simulations Flux 2-D, Flux 3-D, or Inca 3-D have been run to compute these parameters. However, these simulations are highly time-consuming (days up to weeks in 3-D configuration) and cannot manage all of the details (e.g., spiral form of the inductors). Consequently, measurements were achieved for the real and imaginary parts of the global impedances including the coupling terms. A specific measurement procedure based on the “pseudoenergy” method from V and I measurements as previously described in [11] for a 1500-Hz resonant frequency leads to the values of the impedance matrix that are given by (4) in milliohms

$$\bar{Z} = \begin{bmatrix} 33.1 + 244.7i & 25.9 + 43.8i & 21.5 + 24.3i \\ 25.8 + 43.6i & 67.3 + 247.3i & 65.9 + 113.7i \\ 20.9 + 21.4i & 65.2 + 111.4i & 107.1 + 568.2i \end{bmatrix} \quad (4)$$

In order to reach a flat temperature profile in the heated metal sheet according to the principles presented in [8]–[10], the reference currents have to be optimized through an optimization procedure. One of the best combinations of the supply currents

TABLE I
BEST SETTINGS FOR A FLAT TEMPERATURE PROFILE

I1(A)	I2(A)	φ_{21} (°)	I3(A)	φ_{31} (°)
253.9	114.7	-49.4	92.8	-63.1

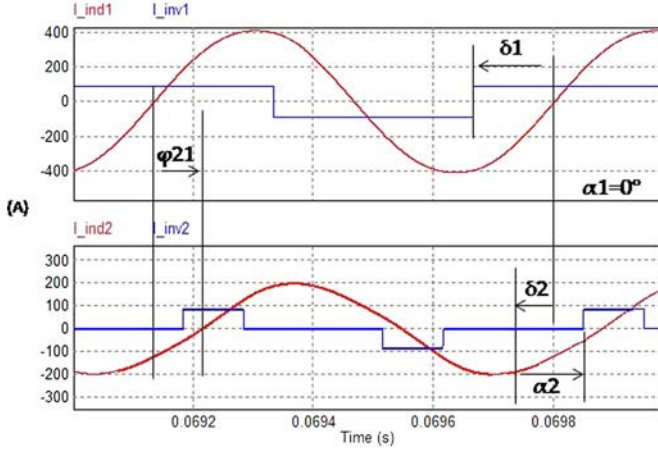


Fig. 4. Phase 1 and 2 inverter and inductor waveforms.

is recalled in Table I for a required power density distribution of 10 MW/m^3 in a 0.45 radius disc made of stainless steel. The current waveforms for the inverter currents and the inductor currents are shown in Fig. 4 for phases 1 and 2 as an example, with their characteristic angles for each phase i ($\alpha_i, \delta_i, \varphi_{ij}$). Consequently, the current controllers will have to adjust the duty cycle α_i on each phase and the phase lag φ_{ij} between the inductor currents in order to follow the inductor sinusoidal reference currents.

III. RESONANT CURRENT CONTROL

Initially proposed in [12], resonant controllers have very interesting properties when sinusoidal references of multiple frequencies have to be controlled as in [13]. Resonant controllers can achieve a high performance in both multisinusoidal reference tracking and disturbance rejection owing to an infinite gain at the fundamental frequency. There is no matrix transformation such as Park's transformation in these controllers! Consequently, the control scheme is simpler, and the computational burden is reduced. Some tuning methods can be found for such controllers; they are mainly based on Bode diagram and pole-zero map. Interesting as they may be, these methods do not take into account the time behavior of the system since they mainly involve phase or gain margins. Moreover, they only deal with single-phase systems; nothing can be found for multiphase systems. The general form of a resonant controller can be expressed in the s -domain as in (5), where $h\omega$ is the h th harmonic to track and ξ is a damping factor (set to zero in this case). Parameters a , b , and c must to be tuned in order to fulfill the desired transients and stability. Moreover, [14] gives a general method to tune a , b , and c for robust control. It has been successfully applied in [15] for the control of a seven-phase synchronous machine. The simplest

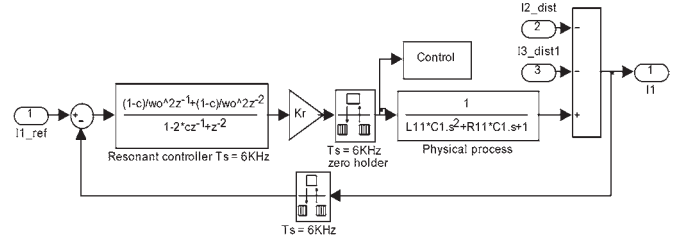


Fig. 5. Block diagram for one phase and resonant controller in z -domain.

resonant controller can be expressed in (6) for the continuous form and (7) for the discrete transfer function

$$G(s) = \frac{a + bs + cs^2}{s^2 + \frac{2\xi}{h\omega}s + (h\omega)^2} \quad (5)$$

$$C_R(s) = \frac{K_r}{s^2 + \omega_0^2} \quad (6)$$

$$C_R(z) = \frac{K_r [1 - \cos(\omega_0 T_s)] (z^{-1} + z^{-2})}{\omega_0^2 z^{-2} - 2z^{-1} \cos(\omega_0 T_s) + 1} \quad (7)$$

ω_0 is the frequency of the sinusoidal reference, and T_s is the sampling period. Fig. 5 presents the block diagram for phase 1, for example, with its discrete resonant controller, while Fig. 6 describes the whole three-phase system with the coupling terms.

A simple closed-loop transfer function can be written in (8) without including the disturbance measurements I_2 and I_3 for the calculation of the control of current I_1 , for example, in Fig. 4. Nevertheless, the coupling effects will be included in the simulation model and of course in the experiments. The characteristic equation derives from (8) and leads to a stability condition using the Routh–Hurwitz criterion in s -domain in (9). The conclusion is in (10)

$$\frac{I_1(z)}{I_{1ref}(z)} = \frac{K_r C_R(z) H(z)}{1 + K_r C_R(z) H(z)} \quad (8)$$

$$(s^2 + \omega_0^2) (L_{11} C_1 s^2 + R_{11} C_1 s + 1) + K_r = 0 \quad (9)$$

$$-\omega_0^2 < K_r < 0. \quad (10)$$

However, as stability is hard to achieve with only one tuning parameter in the z -domain, a more general form of the resonant controller was used in our precedent paper [16]. The corresponding discrete transfer function was given by (11). Under this form, two parameters (K_{r1} and K_{r2}) must be tuned on each phase

$$C_R(z) = \frac{1 [1 - \cos(\omega_0 T_s)] (K_{r1} z^{-1} + K_{r2} z^{-2})}{\omega_0^2 z^{-2} - 2z^{-1} \cos(\omega_0 T_s) + 1}. \quad (11)$$

However, stability can be achieved only with K_{r1} (with K_{r2} equal to 0), and the search of the stable points will be easier. The corresponding discrete form of the reduced resonant controller is given by

$$C_R(z) = \frac{K_r z^{-1}}{z^{-2} - 2z^{-1} \cos(\omega_0 T_s) + 1}. \quad (12)$$

Our precedent papers looked for the point of stability of the three phases separately, without taking into account the coupling effects, i.e., the influence of the \bar{Z}_{ij} terms in (1). On the contrary, this paper searches the stable points of the entire system, including the couplings, by analyzing the norm of the poles in the discrete domain. In Fig. 7, the red points are stable,

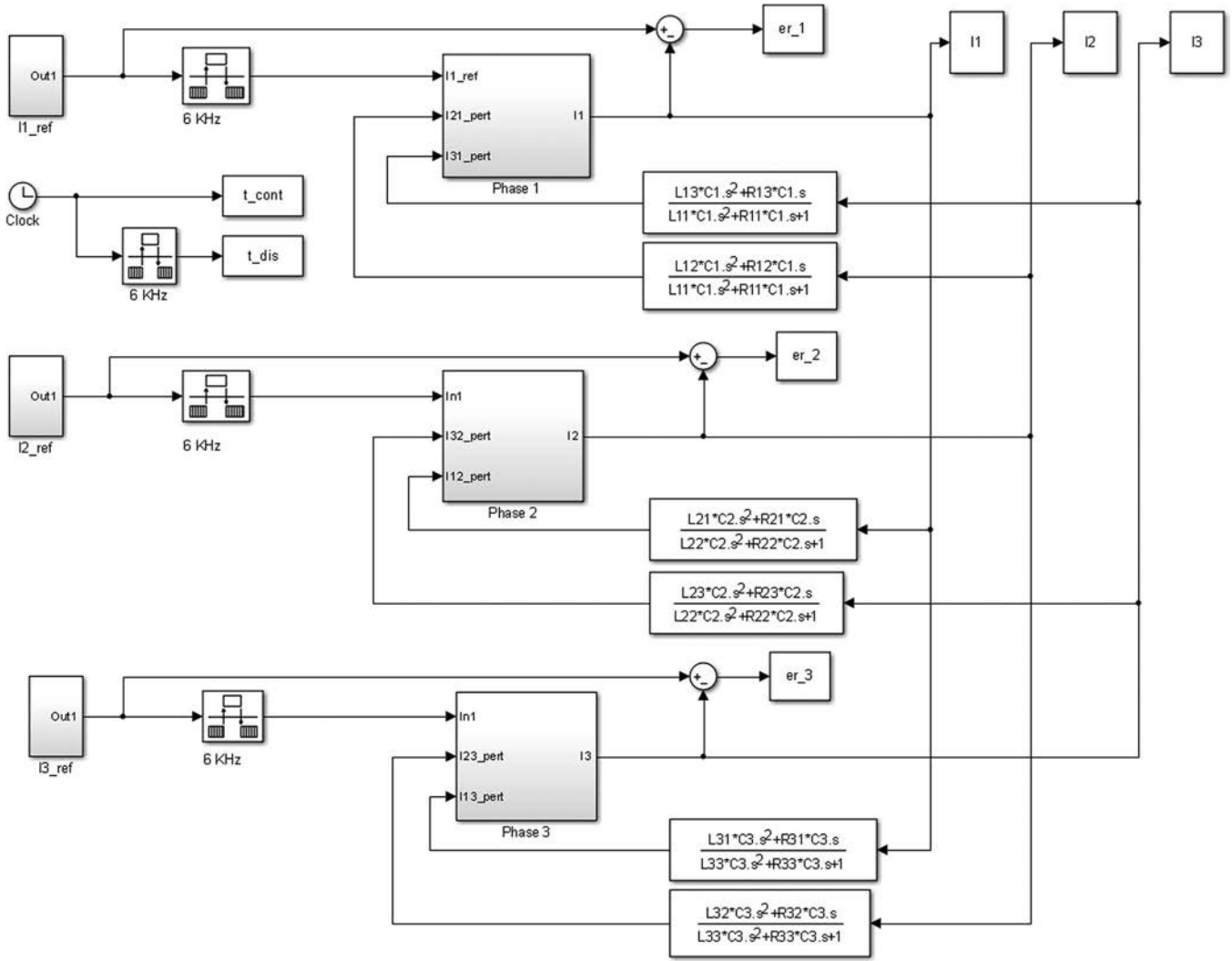


Fig. 6. Three-phase system with coupling and resonant controllers.

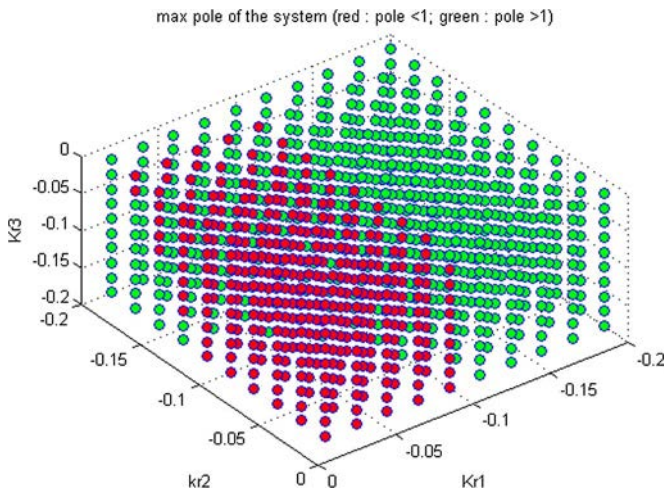


Fig. 7. Maxima of the pole norms versus the resonant controller gains.

and the green ones are unstable. Among the stable points, the points with the smallest norm are chosen and given in Table II.

The corresponding simulated time responses are shown in Figs. 8 and 9 with very low tracking errors (zooms), small overshoot, and reduced time response.

TABLE II
OPTIMAL GAINS FOR A MINIMUM POLE'S NORM

K_{r1}	K_{r2}	K_{r3}	Max pole's norm
-0.06	-0.1	-0.02	0.970758

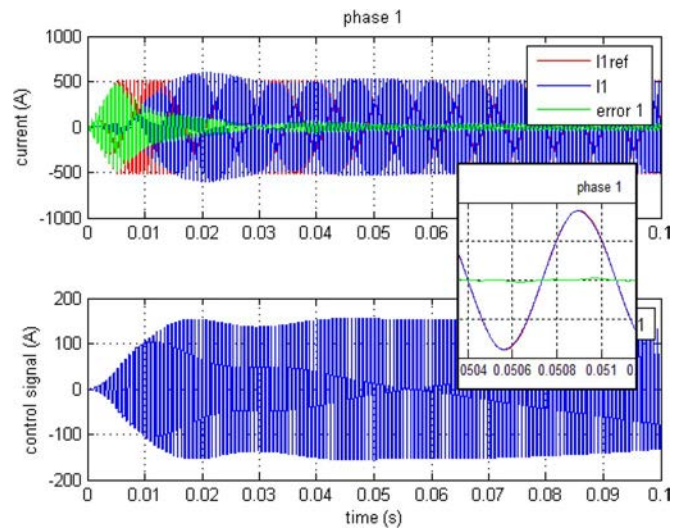


Fig. 8. Reference, output current, error, and control for phase 1.

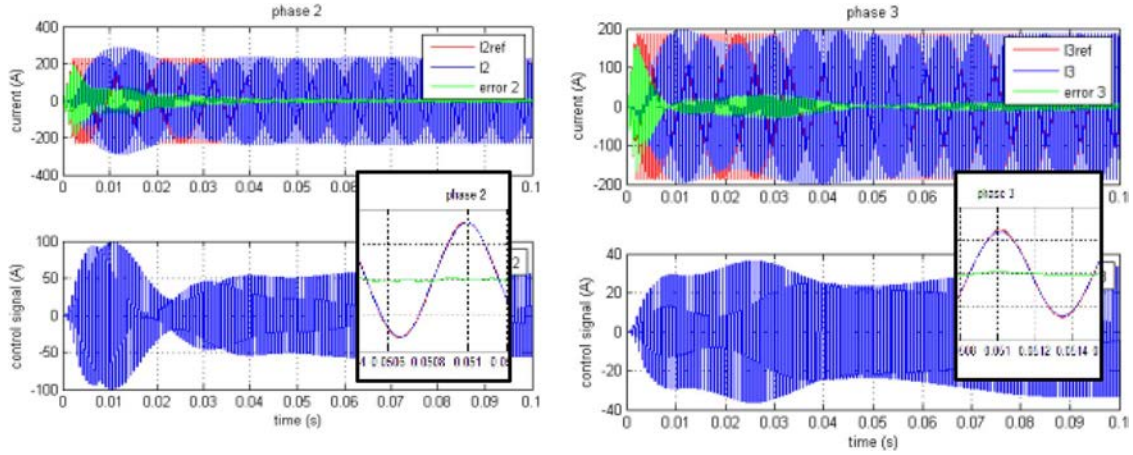


Fig. 9. (a) Reference, output current, and error for phase 2. (b) Reference, output current, and error for phase 3.

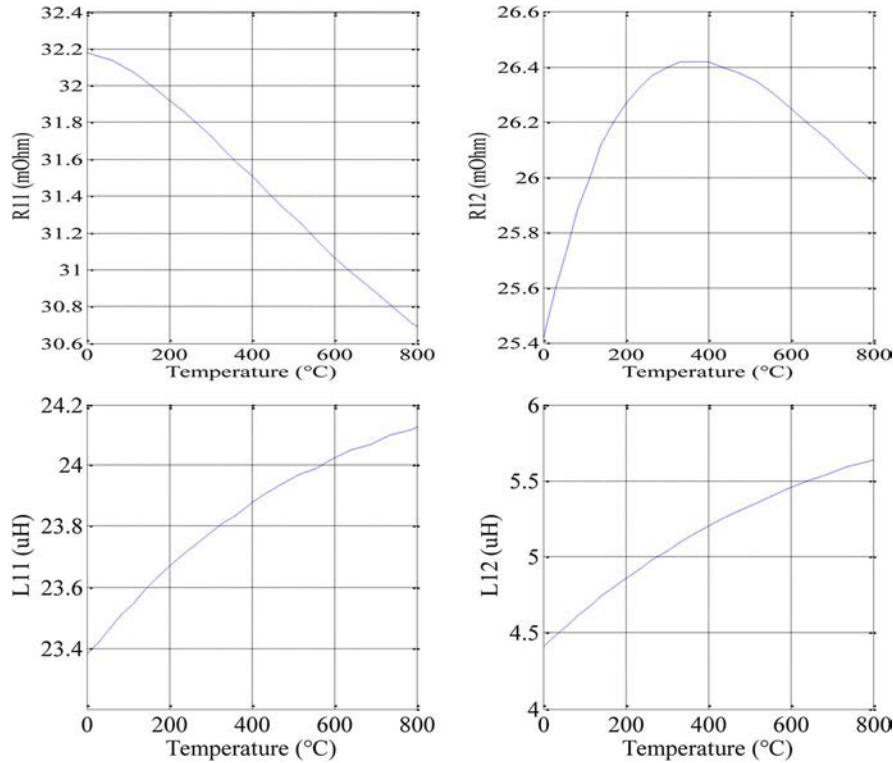


Fig. 10. Examples of parameter variations with temperature. (a) Real and (b) imaginary parts of Z_{ij} .

IV. ROBUSTNESS STUDY

The robustness of the system versus temperature has been simulated in the following part. Few papers deal with these considerations and even less in the case of multiphase systems. Indeed, since the stainless steel is heated, the R_4 term in Z_{ii} and Z_{ij} terms will vary. Nevertheless, some papers such as [17] are focused on the effect of temperature dependence of magnetic properties on the heating characteristics of the $B-H$ curves for a billet heater. Moreover, it is claimed in [18] that temperature has no significant effect around 250 °C in the field of domestic appliances. Carretero *et al.* present in [19] a comprehensive study of the temperature and frequency influence on parameters (R, L) for single-phase domestic induction heating appliances. It is shown that temperature has a limited but nonlinear effect on the $R-L$ parameters (max 0.2%/°C), but the system does

not include the potential impact on control. This paper also points out that the metal resistivity increases with temperature and highly influences the temperature profile around 700 °C. Galunin *et al.* indicate in [20] that temperature-dependent material properties (with $Cv = Cv(T)$ being the volume specific heat of the strip material and $\lambda = \lambda(T)$ being its thermal conductivity) are taken into account at each time step. Parameters are corrected according to the temperature distribution in the workpiece at the previous time step, but no global temperature effect is given. Consequently, it is hard to conclude especially in multiphase systems. From our study, Fig. 10 shows the computed evolution of some Z_{ij} parameters as examples. It can be noticed that the shapes as well as the evolution rates are quite different from one to another under temperature variations in (2) and (3) through resistivity variations.

TABLE III
SIMULATION INDUCTOR CURRENT VARIATIONS VERSUS TEMPERATURE

	25°C	200°C	400°C
I_{1max} (A)	356	356.2	357.4
I_{2max} (A)	177.7	174.4	170
I_{3max} (A)	130.3	127.4	125.9
$\phi_{i_{21}}$ (°)	-41	-38.77	-39.07
$\phi_{i_{31}}$ (°)	-60	-63.04	-67.13

TABLE IV
 Z_{ij} PARAMETER MODEL VARIATIONS VERSUS TEMPERATURE

	25°C	200°C	400°C
R11	0.0361342	0.0357361	0.0350717
R12	0.0285181	0.0292606	0.0294212
R13	0.0221604	0.0234023	0.0240771
R21	0.0285182	0.0292606	0.0294212
R22	0.0774011	0.0785965	0.0783802
R23	0.0752367	0.0767747	0.0767368
R31	0.0221604	0.0234023	0.0240771
R32	0.0752367	0.0767747	0.0767368
R33	0.1255237	0.1245204	0.1218217
X11	0.2221155	0.2248484	0.2274146
X12	0.0411916	0.0451211	0.0490916
X13	0.0194469	0.0227600	0.0262654
X21	0.0411916	0.0451211	0.0490916
X22	0.2427039	0.2527126	0.2627150
X23	0.1096059	0.1204098	0.1312485
X31	0.0194469	0.0227601	0.0262654
X32	0.1096059	0.1204098	0.1312485
X33	0.5706973	0.5854738	0.5997476

TABLE V
CLOSED-LOOP POLE AND ZERO VARIATIONS VERSUS TEMPERATURE

Phase 1	Poles 1,2	Poles 3, 4	Zeros
25°C	$0.0445 \pm 0.9435i$	$-0.0386 \pm 0.9368i$	1; -0.9022
200°C	$0.0464 \pm 0.9446i$	$-0.0405 \pm 0.938i$	1; -0.9052
400°C	$0.0486 \pm 0.9459i$	$-0.0426 \pm 0.9403i$	1; -0.9086

Phase 2	Poles 1,2	Poles 3, 4	Zeros
25°C	$-0.0711 \pm 0.886i$	$0.0767 \pm 0.887i$.7613; 0.75
200°C	$-0.0748 \pm 0.8917i$	$0.0804 \pm 0.8889i$.7699; 0.75
400°C	$-0.0803 \pm 0.8963i$	$0.0859 \pm 0.8921i$.7813; 0.75

Phase 3	Poles 1,2	Poles 3, 4	Zeros
25°C	$0.0674 \pm 0.9272i$	$-0.0617 \pm 0.9145i$	1; -0.8546
200°C	$0.0704 \pm 0.9272i$	$-0.0646 \pm 0.9145i$	1; -0.8611
400°C	$0.074 \pm 0.9316i$	$-0.0682 \pm 0.9213i$	1; -0.8687

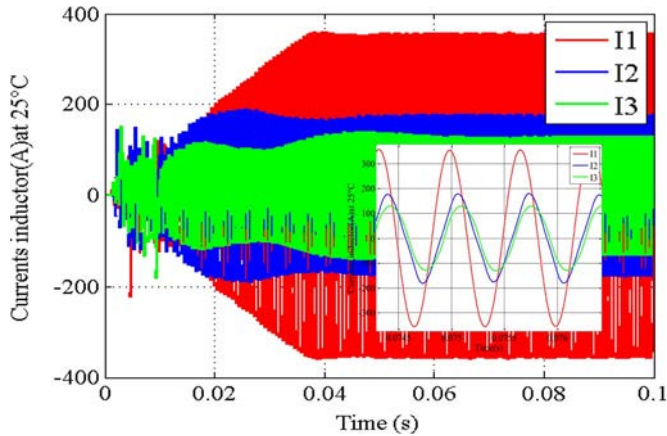


Fig. 11. Closed-loop simulated inductor currents at 25 °C.

Since the Z_{ij} parameter variations may influence the model, their impact is checked, as depicted in Table III for the currents, in Table IV for the Z_{ij} parameters, and in Table V where

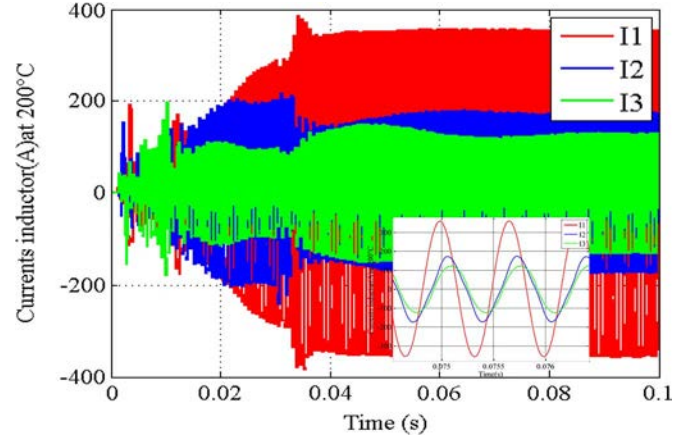


Fig. 12. Closed-loop simulated inductor currents at 200 °C.

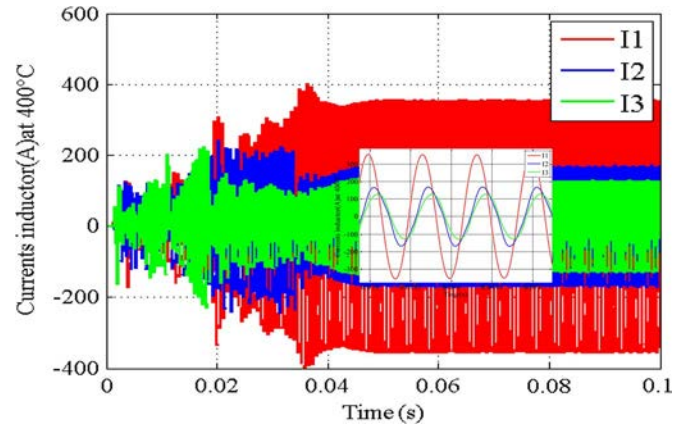


Fig. 13. Closed-loop simulated inductor currents at 400 °C.

TABLE VI
EXPERIMENTAL INDUCTOR CURRENTS VERSUS TEMPERATURE

	reference	25°C	120°C	250°C
I_{1max} (A)	269.3	281.4	281.4	281.4
I_{2max} (A)	121.5	128.4	130.1	130.9
I_{3max} (A)	98.2	100.8	101.5	102.3
$\Phi_{i_{21}}$ (°)	-49.4	-47.1	-47.3	-47.6
$\Phi_{i_{31}}$ (°)	-63.1	-61.1	-61.7	-61.8

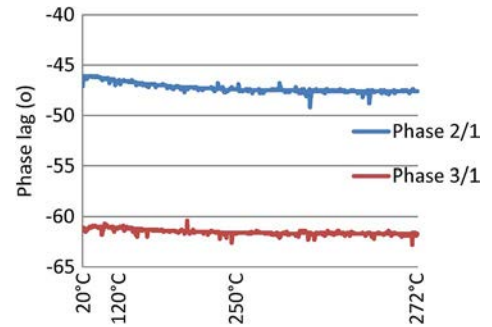


Fig. 14. Closed-loop experimental evolution of the inductor current phase lags with temperature.

the pole-zero variations in the closed-loop transfer functions are listed. Despite these parameter variations, the resonant controllers achieve a good steady-state tracking control of the inductor currents in this three-phase system, as shown in Figs. 11–13 and Table III for three temperatures (25 °C, 200 °C, and 400 °C).

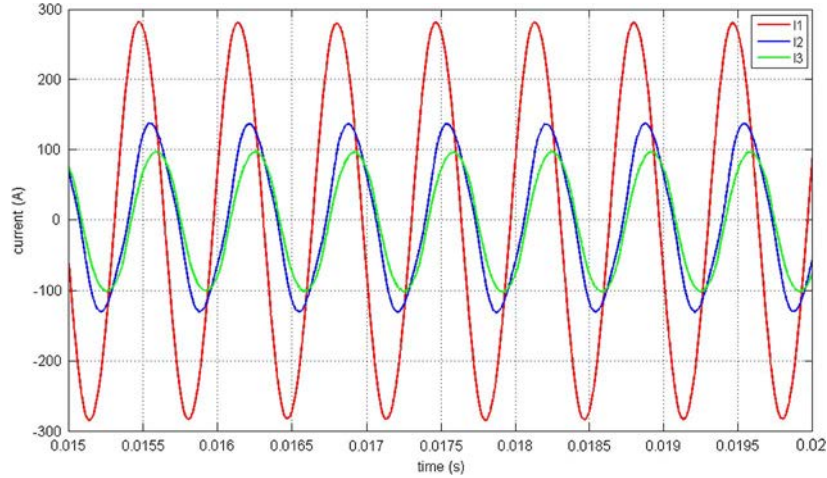


Fig. 15. Closed-loop experimental inductor currents at 20 °C.

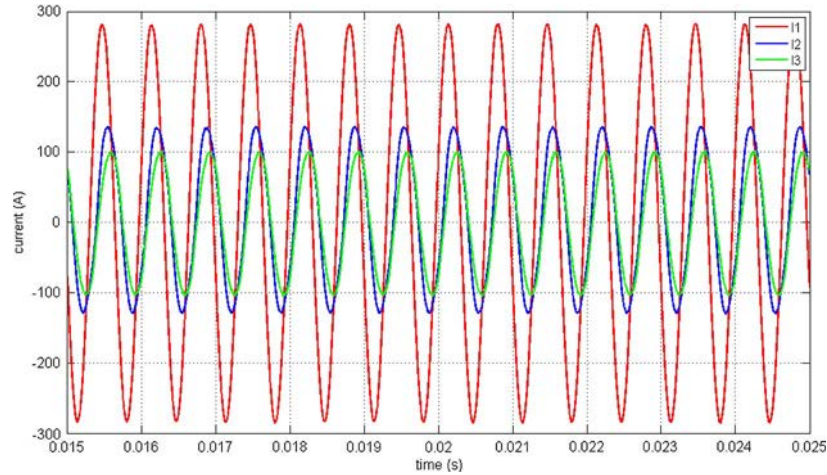


Fig. 16. Experimental inductor currents in the closed loop at 280 °C.

Table VI summarizes the simulated closed-loop currents at different operating temperatures obtained with the resonant controllers as previously tuned. It can be seen that these variations remain rather low during either transients or steady states owing to the good performance of the resonant controllers which track the inductor currents close to their sinusoidal references. Finally, the pole norm calculation such as in Fig 5 can be launched again for several temperatures. The minimum solutions obtained in each of these different cases, leading for the minimum norm of the closed-loop poles, are all the same, which put in evidence the robustness of the system.

With a precise given impedance matrix as in [4], the open-loop control signals have the right characteristics so that the inductor currents have the right amplitudes and phase lags [8]. However, as the impedance matrix changes gradually according to the temperature, a predetermination strategy is impossible, and the resonant controllers will help in achieving precise current control. Fig. 14 shows the evolution of the phase lags of the closed-loop inductor currents. The effects of the temperature rise on the current shapes remain quite low as seen in Figs. 15 and 16, where the experimental inductor currents in the closed loop can be found for two temperatures 20 °C and 280 °C. In that case, the amplitude of the reference inductor current was reduced to 3/4 of the values given in Table III in order to avoid current

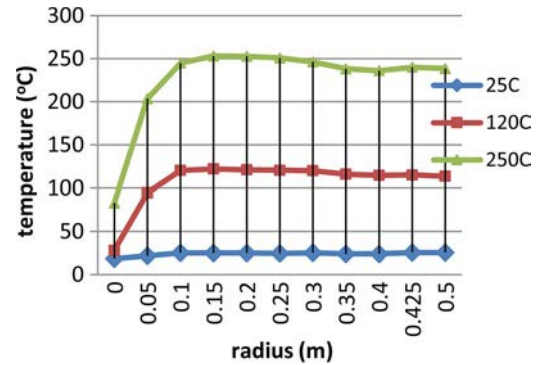


Fig. 17. Experimental temperature profiles in the closed loop.

sensor saturation (cf., Table IV). Either constant amplitudes and phase lags or low distortion from one to another are achieved.

Fig. 17 shows the temperature profile around 25 °C, 120 °C, and 250 °C at 11 points along one radius of the metal disc during heating. Fig. 18 gives a thermal image of the metal disc at the end of the heating. It can be seen as a rather homogenous temperature (except at the center of the disc of course) which confirms the good behavior of the current controllers and their ability to reach the optimal settings in order to heat the disc homogeneously.

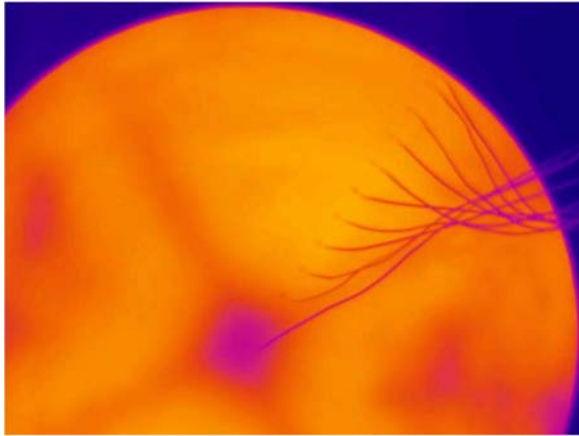


Fig. 18. Experimental metal disc under thermal camera at 250 °C.

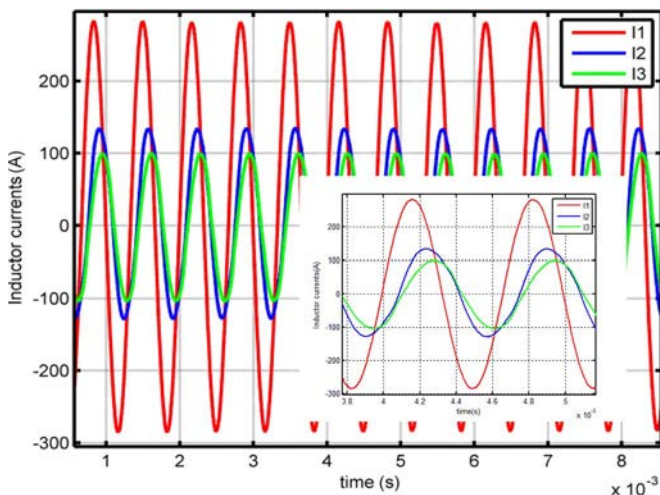


Fig. 19. Experimental inductor currents at 278 °C and 5-cm disc shift.

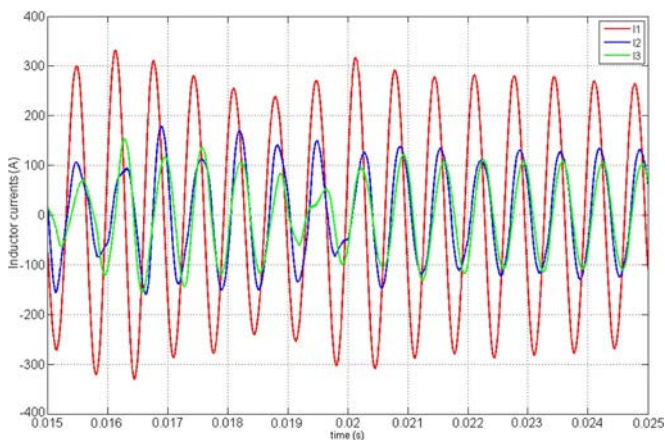


Fig. 20. Experimental inductor currents at 150 °C and 10-cm disc shift.

Moreover, once the inductor currents are well controlled, robustness is tested by displacing the center of the metal disc by 5 cm and 10 cm. With 5-cm displacement, the currents remain well controlled up to 278 °C, as seen in Fig. 19, which is quite similar to Fig. 13 or 14 where the disc is at the center of the system. However, with a 10-cm shift, the currents are modified at about 150 °C in Fig. 20.

V. CONCLUSION

This paper has presented a robustness study of a multiphase induction heating system with controlled currents with the help of resonant controllers. It achieves a rather good behavior either in transients or steady states despite the coupling effects between the phases and with the load, which act as disturbances. Temperature rise has a low impact on the current control and on the temperature distribution in the metal sheet. In order to reduce the temperature profile variations, temperature closed loop will be studied in future work. Additionally, the current transient control will be another interesting issue.

ACKNOWLEDGMENT

The authors would like to thank P. Texeira from EDF R&D for his contribution and the third year ENSEEIHT students in electrical engineering and control, K. Bunthern, V. Forgues-Doumenjou, A. Giani, H. T. Leluong, and F. Salameh, for their valuable participation during their 2013 internship.

REFERENCES

- [1] T. Tudorache and V. Fireteanu, "Magneto-thermal-motion coupling in transverse flux heating," *COMPEL, Int. J. Comput. Math. Elect. Electron. Eng.*, vol. 27, no. 2, pp. 399–407, 2008.
- [2] Y. Neau *et al.*, "High power transverse flux inductor for industrial heating," in *Proc. Electromagn. Properties Mater. Conf.*, 2003, pp. 570–575.
- [3] O. Fishman and N. Vladimír, "Gradient induction heating of a work-piece," U.S. Patent 20 090 314 768, Dec. 24, 2009.
- [4] H. Fujita, N. Uchida, and K. Ozaki, "Zone controlled induction heating (ZCIH)—A new concept in induction heating," in *Proc. Power Convers. Conf.*, 2007, pp. 1498–1504.
- [5] H. N. Pham, H. Fujita, K. Ozaki, and N. Uchida, "Dynamic analysis and control for resonant currents in a zone-control induction heating system," *IEEE Trans. Power Electron.*, vol. 28, no. 3, pp. 1297–1307, Mar. 2013.
- [6] N. Uchida, K. Kawanaka, H. Nanba, and K. Ozaki, "Induction heating method and unit," U.S. Patent 2 007 012 577, Jun. 7, 2007.
- [7] B. You, P. Xu, J. Wang, and G. Zhang, "Power control of induction heating inverse power supply," in *Proc. Int. Conf. Meas., Inf. Control*, 2012, vol. 2, pp. 809–812.
- [8] J. Egalon, S. Caux, P. Maussion, M. Souley, and O. Pateau, "Multi phase system for metal disc induction heating: Modeling and rms current control," *IEEE Trans. Ind. Appl.*, vol. 48, no. 5, pp. 1692–1699, Sept/Oct. 2012.
- [9] M. Souley, S. Caux, O. Pateau, P. Maussion, and Y. Lefèvre, "Optimization of the settings of multiphase induction heating system," in *Conf. Rec. IEEE IAS Annu. Meeting*, 2012, pp. 1–6.
- [10] M. Souley *et al.*, "Optimization of the settings of multiphase induction heating system," *IEEE Trans. Ind. Appl.*, vol. 49, no. 6, pp. 2444–2450, Nov./Dec. 2013.
- [11] M. Souley *et al.*, "Methodology to characterize the impedance matrix of multi-coil induction heating device," in *Proc. Electromagn. Properties Mater. Conf.*, 2009, pp. 201–204.
- [12] Y. Sato, T. Ishizuka, K. Nezu, and T. Kataoka, "A new control strategy for voltage-type PWM rectifiers to realize zero steady-state control error in input current," *IEEE Trans. Ind. Appl.*, vol. 34, no. 3, pp. 480–486, May/Jun. 1998.
- [13] A. G. Yepes, F. D. Freijedo, O. López, and J. Doval-Gandoy, "Analysis and design of resonant current controllers for voltage-source converters by means of Nyquist diagrams and sensitivity function," *IEEE Trans. Ind. Electron.*, vol. 58, no. 11, pp. 5231–5250, Nov. 2011.
- [14] J. Zeng, P. Degobert, D. Lorient, and J. P. Hautier, "Robust design of the self-tuning resonant controller for ac current control systems," in *Proc. IEEE Int. Ind. Technol. Conf.*, 2005, pp. 783–788.
- [15] X. Kestelyn, Y. Crevits, and E. Semail, "Auto-adaptive fault tolerant control of a seven-phase drive," in *Proc. IEEE Int. Ind. Electron. Symp.*, 2010, pp. 2135–2140.
- [16] K. L. Nguyen, S. Caux, X. Kestelyn, O. Pateau, and P. Maussion, "Resonant control of multi-phase induction heating systems," in *Proc. IEEE Ind. Electron. Conf.*, 2012, pp. 3293–3298.

- [17] H. Kagimoto, D. Miyagi, N. Takahashi, N. Uchida, and K. Kawanaka, "Effect of temperature dependence of magnetic properties on heating characteristics of induction heater," *IEEE Trans. Magn.*, vol. 46, no. 8, pp. 3018–3021, Aug. 2010.
- [18] M. Zlobina *et al.*, "Numerical modeling of non-linear transverse flux heating systems," in *Int. Sci. Colloq., Model. Electromagn. Process.*, 2003, pp. 51–56.
- [19] C. Carretero, J. Acero, R. Alonso, J. M. Burdio, and F. Monterde, "Temperature influence on equivalent impedance and efficiency of inductor systems for domestic induction heating appliances," in *Proc. Appl. Power Electron. Conf.*, 2007, pp. 1233–1239.
- [20] S. Galunin, M. Blinov, and Y. Kirill, "Numerical model approaches for in-line strip induction heating," in *Proc. EUROCON*, 2009, pp. 1607–1610.



Kien Long Nguyen received the M.S. degree in electrical and automatic engineering from the Institut National Polytechnique de Toulouse, Toulouse, France, in 2012.

He is currently with the Laboratoire PLAsma et Conversion d'Énergie (LAPLACE), Toulouse. His research interests include current control methods for induction systems.



Olivier Pateau received the Electrical Engineer degree from the Conservatoire National des Arts et Métiers, Paris, France, in 2004.

He has been with Electricité de France (EDF) R&D, Moret sur Loing, France, since 1996, working in the field of induction heating in industry (modeling, design, testing, etc.).



Stéphane Caux (M'07) was born in 1970. He received the Ph.D. degree in robotics from Montpellier University, Montpellier, France, in 1997.

He has been an Assistant Professor with the Laboratoire d'Electrotechnique et d'Electronique Industrielle (LEEI) and the Laboratoire PLAsma et Conversion d'Énergie (LAPLACE), Toulouse, France, since 1998. His main interests concern robust control and observers for electrical systems (electrical motors, inverters, and fuel cell systems), and real-time energy management for multisource electrical systems (optimization and fuzzy management).



Pascal Maussion (M'07) received the M.Sc. and Ph.D. degrees in electrical engineering from Institut National Polytechnique de Toulouse, Toulouse, France, in 1985 and 1990, respectively.

He is currently a Full Professor with the University of Toulouse, Toulouse, and a Researcher with the Centre National de la Recherche Scientifique Research Laboratory, Laboratoire PLAsma et Conversion d'Énergie (LAPLACE), Toulouse. He is currently the Head of the Control and Diagnosis Research Group, LAPLACE. He teaches courses on

control and diagnosis at the University of Toulouse. His research activities deal with the control and diagnosis of electrical systems such as power converters, drives, and lighting and with the design of experiments for optimization in control and diagnosis.



Julie Egalon received the M.S. degree in electrical engineering from the Institut National Polytechnique de Toulouse, Toulouse, France, in 2009 and the Ph.D. degree from the Laboratoire PLAsma et Conversion d'Énergie (LAPLACE), Toulouse, in 2013.

She is currently an Electrical Engineer with Betem Midi Pyrénées, Toulouse. Her research interests include current control methods for the present induction system.